

# Effect of Ge Concentration on the Microstructure of Germanium Nanocrystals Produced by Ion Implantation in SiO<sub>2</sub>

L. H. Ge<sup>1</sup>, C. Wang<sup>1</sup>, R. S. Cai<sup>1</sup>, W. S. Liang<sup>1</sup>, Y. Q. Wang<sup>1,\*</sup>, G. G. Ross<sup>2</sup>, and D. Barba<sup>2,\*</sup>

<sup>1</sup>College of Physics and The Cultivation Base for State Key Laboratory, Qingdao University, Qingdao 266071, People's Republic of China

<sup>2</sup>INRS-Énergie, Matériaux et Télécommunications, 1650 Boulevard Lionel-Boulet, Varennes, Québec J3X 1S2, Canada

Transmission electron microscopy (TEM) has been used to investigate Germanium nanocrystals (Ge-nc) synthesized by implantation of Ge<sup>+</sup> ions into SiO<sub>2</sub> films grown on (100) Si substrates, followed by thermal annealing at 850 °C. High resolution imaging shows that the diameter, heterogeneity and depth-distribution of the formed Ge-nc increase continuously with the Ge concentration. It is evidenced that the biggest Ge-nc form in the sample region where the concentration of implanted Ge is the highest, resulting in a highly size-selective depth-distribution of Ge-nc. By comparing TEM observations with the implanted ion distributions, we show that the formation of Ge-nc larger than 1 nm occurs for Ge concentration greater than  $\sim 5 \times 10^{20}$  Ge<sup>+</sup>/cm<sup>3</sup> ( $\sim 1$  at.%) whereas a minimum local density threshold of  $\sim 4 \times 10^{21}$  Ge<sup>+</sup>/cm<sup>3</sup> ( $\sim 8$  at.%) is required to produce Ge-nc bigger than 6 nm. The fraction of Ge found inside Ge-nc decreases from  $\sim 60\%$  to  $\sim 40\%$  in the heavily ion implanted sample, due to possible reduction of Ge thermal diffusivity in the highly damaged SiO<sub>2</sub> layer. In addition to demonstrate the possible synthesis of Ge-nc in silicon oxide matrices containing Ge concentration as low as 1 at.%, these results enable to directly connect the geometry and the density of the formed nanocrystallites with the germanium concentration, for both the optimization and the control of the Ge-nc synthesis process.

**Keywords:** Ge Nanocrystals, Ion Implantation, TEM, HRTEM.

## 1. INTRODUCTION

Silicon (Si) and germanium nanocrystals (Ge-nc) embedded in silicon dioxide (SiO<sub>2</sub>) or germanosilicate glass have been widely used as efficient light emitters and optical absorbers for many applications in optical sensing technology, memory storage, photonics and photovoltaics.<sup>1–5</sup> Recently, a more specific attention has been paid to Ge-nc for developing new integrated optoelectronic devices and high efficient solar cells,<sup>6,7</sup> where both the size and the crystallinity of the formed nanocrystallites can drastically affect their performances.

Until now, direct characterizations of Ge-nc embedded in SiO<sub>2</sub> by transmission electron microscopy (TEM)<sup>8–12</sup> and atomic force microscopy (AFM)<sup>13,14</sup> have revealed the formation of Ge-nc inside SiO<sub>2</sub>/Si systems, but few of them enable to study simultaneously the evolution of

their size, size-dispersion and spatial distribution as a function of the fabrication parameters. Also, no direct correlation has been clearly established between the synthesis of Ge-nc, their morphology and the local concentration of Ge. These investigations are indispensable for controlling the nature of the formed Ge-nc and tuning their physical properties, especially for nanocrystallites having dimension lower than the germanium Bohr radius.<sup>15</sup> Also, the minimum Ge concentration required for producing Ge-nc is unknown and needs to be estimated in order to determine if the nucleation of Ge can occur in other SiO<sub>2</sub>-based systems such as Ge-doped silica glass entering within the fabrication of numbered optical components. To this end, Ge-nc are produced using a process based on ion implantation which provides an excellent control of the Ge density inside the host matrix compared to other synthesis techniques based on GeO<sub>2</sub> reduction,<sup>9</sup> laser ablation,<sup>16</sup> magnetron-sputtering

\*Authors to whom correspondence should be addressed.

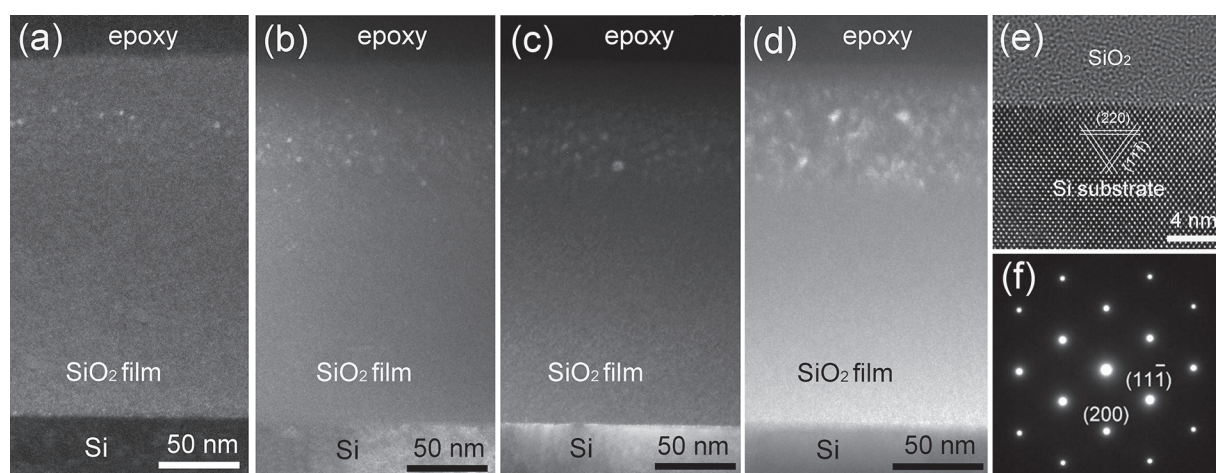


**Figure 1.** Typical dark-field images of the samples implanted at  $1 \times 10^{16}$  Ge<sup>+</sup>/cm<sup>2</sup> (a),  $2 \times 10^{16}$  Ge<sup>+</sup>/cm<sup>2</sup> (b),  $4 \times 10^{16}$  Ge<sup>+</sup>/cm<sup>2</sup> (c),  $8 \times 10^{16}$  Ge<sup>+</sup>/cm<sup>2</sup> (d). Right, HRTEM image of the SiO<sub>2</sub>/Si interface (e), with the [011] zone-axis SAED pattern obtained from the Si substrate (f).

deposition,<sup>17</sup> chemical vapor deposition,<sup>18,19</sup> and molecular beam epitaxy.<sup>5</sup>

In this paper, we present a detailed characterization of Ge-nc thermally synthesized inside SiO<sub>2</sub>/Si systems implanted at ion fluencies of  $1 \times 10^{16}$ ,  $2 \times 10^{16}$ ,  $4 \times 10^{16}$  and  $8 \times 10^{16}$  Ge<sup>+</sup>/cm<sup>2</sup>. We chose an annealing temperature

of 850 °C, giving a representative description of Ge-nc produced from an annealing conducted below the Ge melting point of 938 °C. In such conditions, it was found that Ge desorption effects are negligible and the formed Ge nanocrystallites are highly-ordered.<sup>20,21</sup> The size, size-dispersion and depth-distribution of Ge-nc are measured by

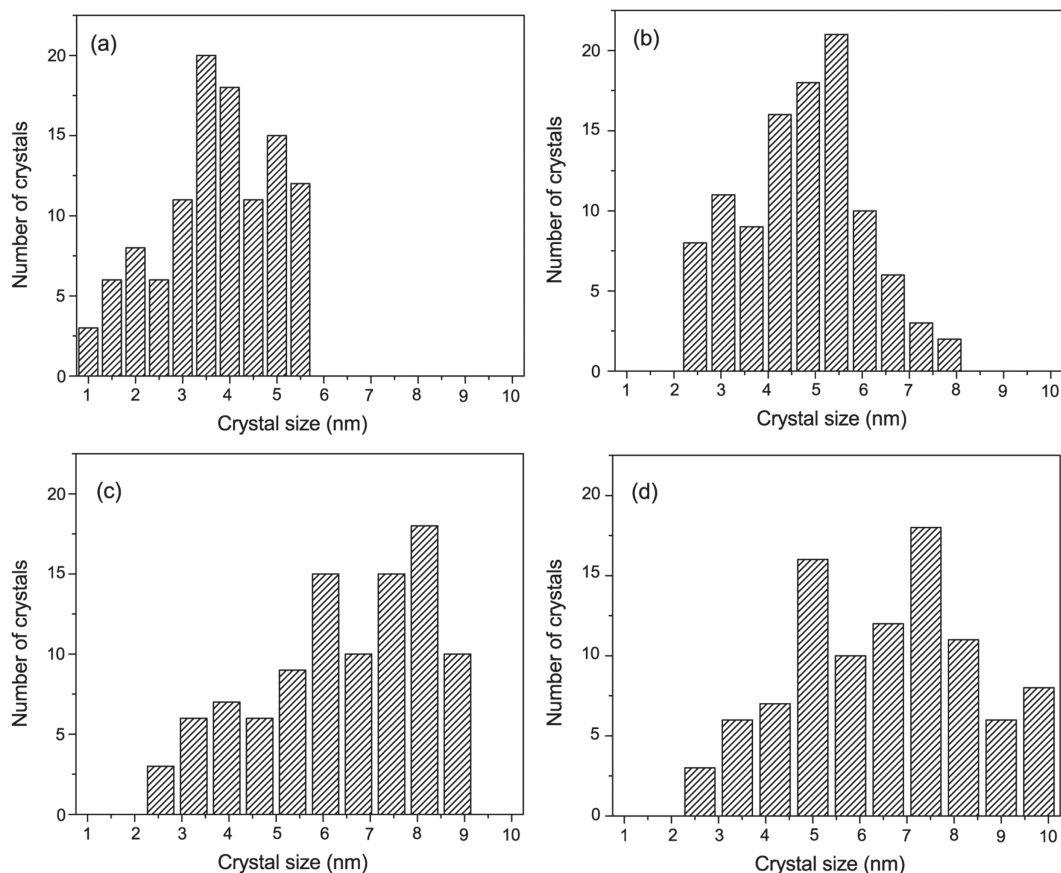


**Figure 2.** Size-distributions of Ge-nc observed by dark-field TEM imaging for samples implanted at  $1 \times 10^{16}$  Ge<sup>+</sup>/cm<sup>2</sup> (a),  $2 \times 10^{16}$  Ge<sup>+</sup>/cm<sup>2</sup> (b),  $4 \times 10^{16}$  Ge<sup>+</sup>/cm<sup>2</sup> (c),  $8 \times 10^{16}$  Ge<sup>+</sup>/cm<sup>2</sup> (d).

**Table I.** Average size, size-dispersion and spatial distribution of Ge-nc.

Implantation dose (cm <sup>-2</sup> )	Starting depth (nm)	Implanted layer thickness (nm)	Average size (nm) Standard deviation
1 × 10 <sup>16</sup>	20 ± 5	53 ± 5	D = 3.71, σ = 0.93
2 × 10 <sup>16</sup>	15 ± 3	55 ± 5	D = 4.74, σ = 1.33
4 × 10 <sup>16</sup>	10 ± 2	58 ± 5	D = 6.42, σ = 1.46
8 × 10 <sup>16</sup>	6 ± 2	64 ± 3	D = 6.50, σ = 2.68

TEM, which allows us to determine the minimum concentration of implanted Ge needed to activate the nucleation of Ge-nc, as well as the fraction of implanted Ge participating in this process. We show that the spatial distribution of the produced Ge-nc is size-selective and strongly connected with the depth profiles of implanted Ge ions within SiO<sub>2</sub> matrix, as well as the possibility of producing Ge-nc in systems containing a Ge concentration as low as 1 at.%.

## 2. EXPERIMENTAL DETAILS

200-nm-thick SiO<sub>2</sub> films were produced by dry thermal oxidation of a (100) Si substrate at 1100 °C. These samples were implanted with 70-keV <sup>74</sup>Ge<sup>+</sup> at room temperature, followed by a thermal annealing at 850 °C (below the melting point of Ge) for 1 h under an atmosphere of nitrogen (N<sub>2</sub>). To avoid any accidental contamination of the

annealing ambient, the gas flux is filtered using an additional nitrogen purifier. To examine the effect of implantation dose on the microstructure of Ge-nc, different doses of 1 × 10<sup>16</sup>, 2 × 10<sup>16</sup>, 4 × 10<sup>16</sup> and 8 × 10<sup>16</sup> cm<sup>-2</sup> were set for the ion implantations.

TEM experiments were carried out on specimens prepared in cross section (oriented along the [011] zone axis of the Si substrates), using conventional techniques of mechanical polishing and ion-thinning. The ion thinning was performed using a Gatan model 691 precision ion polishing system (PIPS). Selected-area electron diffraction (SAED), dark field (DF) imaging and high-resolution TEM (HRTEM) imaging were conducted using a JEOL JEM 2100F TEM operated at 200 kV.

## 3. RESULTS AND DISCUSSION

Typical DF TEM images are shown in Figures 1(a–d) for samples implanted at 1 × 10<sup>16</sup>, 2 × 10<sup>16</sup>, 4 × 10<sup>16</sup> and 8 × 10<sup>16</sup> Ge<sup>+</sup>/cm<sup>2</sup>, respectively. During the acquisition of DF TEM images, all Si substrates were tilted close to the [011] zone-axis in order to obtain a better estimation of the Ge-nc position. These images show clearly the presence of a SiO<sub>2</sub> sublayer containing nanocrystals (bright spots), whose statistical size distribution is presented for

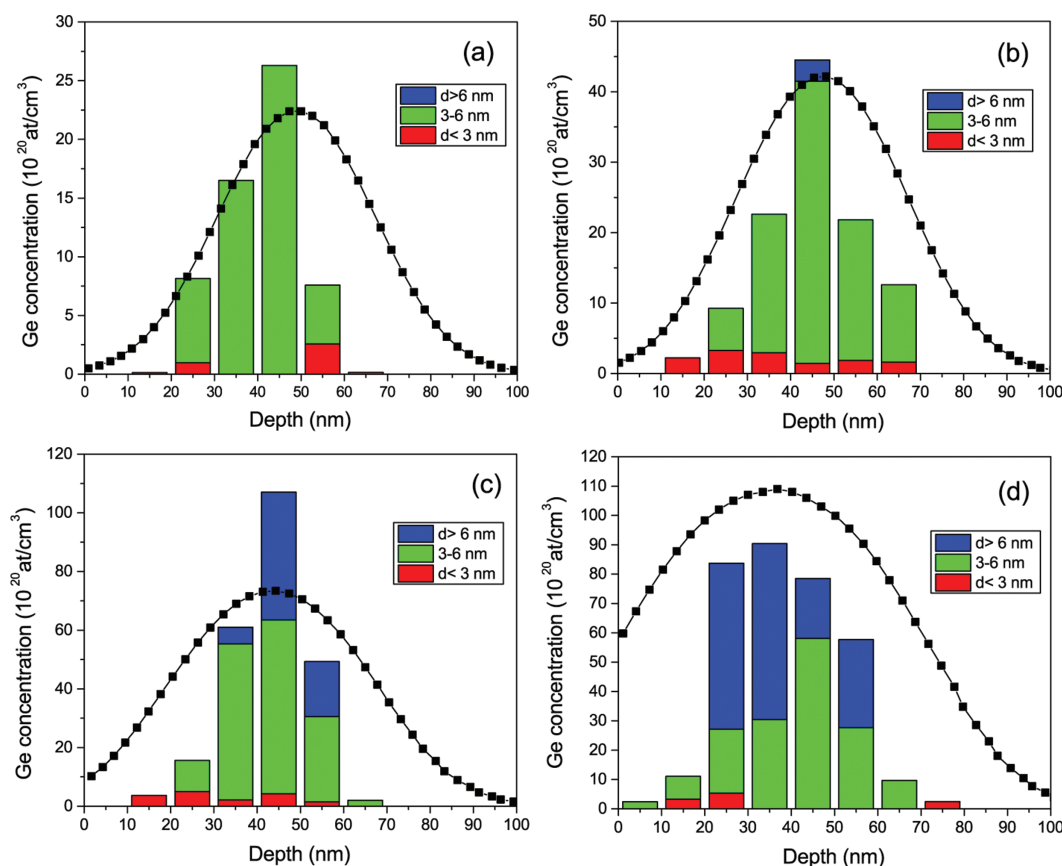


**Figure 3.** SRIM calculated depth-profiles of implanted Ge compared with the depth distribution of the Ge concentration found in Ge-nc, for implantation doses of 1 × 10<sup>16</sup> Ge<sup>+</sup>/cm<sup>2</sup> (a), 2 × 10<sup>16</sup> Ge<sup>+</sup>/cm<sup>2</sup> (b), 4 × 10<sup>16</sup> Ge<sup>+</sup>/cm<sup>2</sup> (c), 8 × 10<sup>16</sup> Ge<sup>+</sup>/cm<sup>2</sup> (d).

each implantation dose in Figures 2(a–d). The starting depth, the thickness of the SiO<sub>2</sub> sublayer containing Ge-nc and the average size of Ge-nc are summarized in Table I. These measurements indicate that the starting depth at which Ge-nc are observed decreases with the implantation dose, while the thickness of the sublayer containing Ge-nc increases continuously. The average size of Ge-nc observed in different samples increases with the implantation dose: from 3.71 nm in the sample implanted at  $1 \times 10^{16}$  Ge<sup>+</sup>/cm<sup>2</sup>, to 6.50 nm in the sample implanted at  $8 \times 10^{16}$  Ge<sup>+</sup>/cm<sup>2</sup>. Such increases of both the Ge-nc sublayer thickness and the Ge-nc dimensions are consistent with the reduction of the spacing between implanted Ge ions at greater implantation doses, which can promote the formation of Ge aggregates into a more extended sample region. For the sample implanted at  $8 \times 10^{16}$  Ge<sup>+</sup>/cm<sup>2</sup>, the average size of the formed Ge-nc (6.50 nm) is quite similar to that measured for Ge-nc synthesized at 850 °C (6.33 nm), 800 °C (6.13 nm) and 700 °C (5.95 nm), reported in Ref. [21].

In Figures 3(a–d), the depth-distributions of Ge found in Ge-nc (classified in three different groups according to their sizes) are compared with the depth profiles of implanted Ge determined by SRIM Monte-Carlo simulations.<sup>22</sup> Both the concentration of Ge-nc and the percentage of Ge that nucleates were reported for each implantation doses in Table II. In these calculations, we assumed that the density of  $4.43 \times 10^{22}$  cm<sup>-3</sup> inside Ge-nc is similar to that of bulk Ge, because the compressive stress exerted by the surrounding SiO<sub>2</sub> on Ge-nc is only of about 2% at this annealing temperature.<sup>21</sup> We took also into account the surface erosion induced by ion sputtering, estimated for each implantation dose using SRIM calculations, as well as the swelling effects related to the introduction of Ge.<sup>22</sup> For the sample implanted at  $8 \times 10^{16}$  Ge<sup>+</sup>/cm<sup>2</sup>, these two effects shift ~25 nm the center position of the implanted Ge depth-profile to the sample surface. The thickness of the TEM specimen is measured to be around 50 nm using electron energy-loss spectroscopy. From the recorded TEM images, we measured Ge-nc concentrations of  $2.67 \times 10^{18}$ ,  $1.94 \times 10^{18}$ ,  $1.75 \times 10^{18}$  and  $1.63 \times 10^{18}$  cm<sup>-3</sup> in the samples implanted at  $1 \times 10^{16}$ ,  $2 \times 10^{16}$ ,  $4 \times 10^{16}$  and  $8 \times 10^{16}$  Ge<sup>+</sup>/cm<sup>2</sup>, respectively, indicating that the formation of bigger Ge-nc is accompanied by an overall reduction of their density inside the SiO<sub>2</sub> layer. The proportion of Ge participating in the growth of Ge-nc remains almost constant around 60% for implantation fluences lower than  $4 \times 10^{16}$  Ge<sup>+</sup>/cm<sup>2</sup>. This percentage drops to 40% in the sample implanted at  $8 \times 10^{16}$  Ge<sup>+</sup>/cm<sup>2</sup>. Such a decrease may result from a significant reduction of the Ge thermal diffusivity inside heavily-damaged SiO<sub>2</sub> layer, where the occurrence of trapping mechanisms between diffusing Ge and Si dangling bonds generated during ion bombardment have already been evoked to explain similar effects observed in fused silica systems implanted with Ge.<sup>23, 24</sup>

**Table II.** Concentration of Ge-nc with percentage of implanted Ge that nucleates.

Implantation dose (cm <sup>-2</sup> )	Concentration of Ge-nc (cm <sup>-3</sup> )	Synthesis efficiency (%)
$1 \times 10^{16}$	$2.67 \times 10^{18}$	63
$2 \times 10^{16}$	$1.94 \times 10^{18}$	61
$4 \times 10^{16}$	$1.75 \times 10^{18}$	60
$8 \times 10^{16}$	$1.63 \times 10^{18}$	43

Typical HRTEM images are shown in Figures 4(a–d) for each sample. Figure 4(e) shows a typical HRTEM image of a single-twin structure, and Figure 4(f) is the HRTEM image of a double-twin structure. Such nanotwins are observed in most Ge-nc with diameters larger than 5 nm. This suggests that the growth mechanisms involved in Ge-nc nucleation are related to Ostwald ripening and coalescence effects, as for Ge-nc synthesized in fused silica.<sup>25</sup>

Except for the sample implanted at  $1 \times 10^{16}$  Ge<sup>+</sup>/cm<sup>2</sup>, where slight discrepancies are reported due to the small

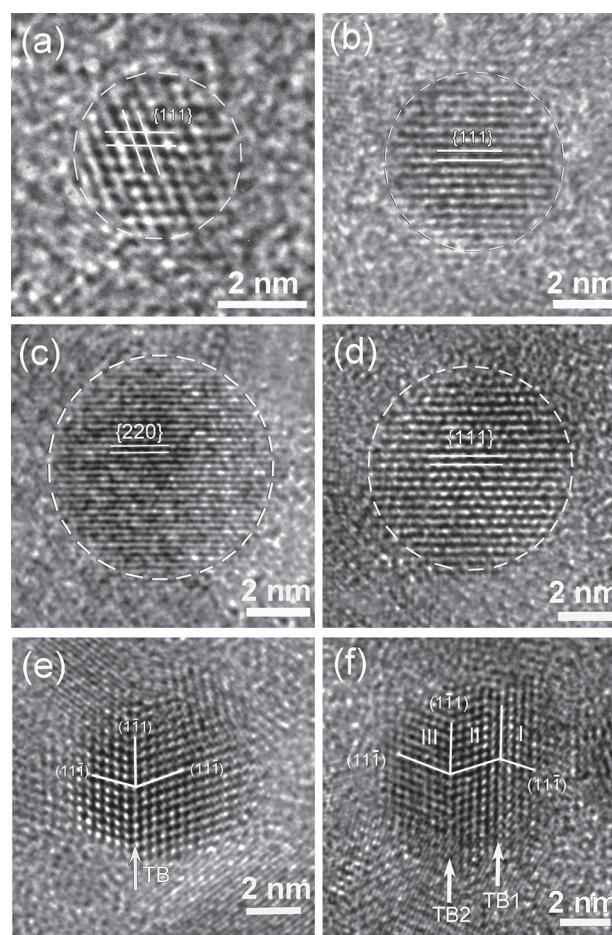


**Figure 4.** HRTEM images of Ge-nc produced from Ge implantation doses of  $1 \times 10^{16}$  Ge<sup>+</sup>/cm<sup>2</sup> (a),  $2 \times 10^{16}$  Ge<sup>+</sup>/cm<sup>2</sup> (b),  $4 \times 10^{16}$  Ge<sup>+</sup>/cm<sup>2</sup> (c),  $8 \times 10^{16}$  Ge<sup>+</sup>/cm<sup>2</sup> (d), with typical HRTEM image of a single-twin structure (e) and a double-twin structure (f).

size of the formed Ge-nc, two remarkable features are evidenced on these figures:

(i) the centering of both the implantation profiles and the profile of observed Ge-nc at the same depth for each ion fluence, and

(ii) the highly size-selective depth-distribution of Ge-nc.

The latter is qualitatively similar to that observed for Si-nc.<sup>25</sup> From a careful examination of these data, we identified three concentration thresholds of implanted Ge, namely  $\sim 5.0 \times 10^{20}$  at·cm<sup>-3</sup> ( $\sim 1.0$  at.%),  $\sim 1.5 \times 10^{21}$  at·cm<sup>-3</sup> ( $\sim 3.0$  at.%), and  $\sim 4.0 \times 10^{21}$  at·cm<sup>-3</sup> ( $\sim 8.0$  at.%), above which, Ge-nc smaller than 3 nm, Ge-nc of 3–6 nm and Ge-nc larger than 6 nm are synthesized, respectively. These three indicative values define the minimum concentration of Ge required for activating the production of Ge nanocrystallites having these specific dimensions during an annealing of 1 h at 850 °C. In addition to quantify the concentration of Ge needed for the synthesis of these Ge-nc, this suggests that the nucleation of Ge-nc can occur at this temperature inside other SiO<sub>2</sub>-based systems containing weak Ge concentration, such as Ge-doped silica glass (where the concentration of Ge-dopant can reach up to 20–30%), which are widely used in optical telecommunication and optical fibre technology.

#### 4. CONCLUSIONS

In summary, a systematic TEM study of Ge-nc produced by ion implantation in SiO<sub>2</sub>/Si systems shows that both the dimension and the size-dispersion of formed nanoclusters increase continuously with the concentration of Ge introduced into the samples. The comparison between the depth-profile of implanted ions and the quantity of Ge found inside Ge-nc reveals that the biggest Ge-nc are produced in the sample region where the local concentration of Ge is the highest. A size-selective depth distribution of Ge-nc is identified by Ge concentration thresholds defining the minimum quantity of Ge needed to form nanocrystals with diameters varying from 1 to 10 nm. We demonstrated that a heating at 850 °C can promote the synthesis of Ge nanocrystallites in SiO<sub>2</sub>-based systems containing a Ge concentration as low as 1 at.%, which is in the order of the Ge content inside Ge-doped silica glass employed in a large variety of optical components, such as optical sensors and fibers. The quantity of implanted Ge participating into the Ge-nc nucleation was estimated between 60 and 40% in the studied samples, indicating a possible reduction of the Ge thermal diffusion in heavily-implanted SiO<sub>2</sub> layers.

**Acknowledgments:** The authors would like to thank the financial support from the National Key Basic Research Development Program of China (Grant no.: 2012CB722705), the 4th Workgroup Québec-Shandong

program, the Natural Science Foundation for Outstanding Young Scientists in Shandong Province, China (Grant no.: JQ201002), and High-end Foreign Experts Recruitment Program (Grant nos.: GDW20143500163, GDW20133400112). Y. Q. Wang would also like to thank the financial support from the Top-notch Innovative Talent Program of Qingdao City (Grant no.: 13-CX-8), and the Taishan Scholar Program of Shandong Province, China.

#### References and Notes

1. L. T. Canham, *Appl. Phys. Lett.* 57, 1046 (1990).
2. Y. Q. Wang, R. Smirani, and G. G. Ross, *Nano Lett.* 4, 2041 (2004).
3. Y. Q. Wang, R. Smirani, and G. G. Ross, *Appl. Phys. Lett.* 86, 221920 (2005).
4. Y. Q. Wang, R. Smirani, G. G. Ross, and F. Schiettekatte, *Phys. Rev. B* 71, 161310R (2005).
5. S. Das, R. K. Singha, K. Das, A. Dhar, and S. K. Ray, *J. Nanosci. Nanotechnol.* 9, 5484 (2009).
6. M. Yedji, J. Demarche, G. Terwagne, R. Delamare, D. Flandre, D. Barba, D. Koshel, and G. G. Ross, *J. Appl. Phys.* 109, 084337 (2011).
7. M. C. Beard, K. P. Knutsen, P. Yu, J. M. Luther, Q. Song, W. K. Metzger, R. J. Ellingson, and A. J. Nozik, *Nano Lett.* 7, 2506 (2007).
8. E. S. Marstein, A. E. Gunnæs, U. Serincan, S. Jørgensen, A. Olsen, R. Turan, and T. G. Finstad, *Nucl. Instrum. Methods B* 207, 424 (2003).
9. W. K. Choi, V. Ho, V. Ng, Y. W. Ho, S. P. Ng, and W. P. Chim, *Appl. Phys. Lett.* 86, 143114 (2005).
10. J. G. Zhu, C. W. White, J. D. Budai, S. P. Withrow, and Y. Chen, *J. Appl. Phys.* 78, 4386 (1995).
11. J. von Borany, R. Grötzschel, K. H. Heinig, A. Markwitz, W. Matz, B. Schmidt, and W. Skorupa, *Appl. Phys. Lett.* 71, 3215 (1997).
12. A. Markwitz, B. Schmidt, W. Matz, R. Grötzschel, and A. Mücklich, *Nucl. Instrum. Methods B* 142, 338 (1998).
13. A. V. Baranov, A. V. Fedorov, T. S. Perova, R. A. Moore, V. Yam, D. Bouchier, V. Le Thanh, and K. Berwick, *Phys. Rev. B* 73, 075322 (2006).
14. J. L. Liu, J. Wan, Z. M. Jiang, A. Khitun, K. L. Wang, and D. P. Yu, *J. Appl. Phys.* 92, 6804 (2002).
15. L. M. Wheeler, L. M. Leij, and U. R. Kortshagen, *J. Phys. Chem. Lett.* 4, 3392 (2013).
16. D. Riabinina, C. Durand, M. Chaker, N. Rowell, and F. Rosei, *Nanotechnology* 17, 2152 (2006).
17. Y. Maeda, *Phys. Rev. B* 51, 1658 (1995).
18. P. Meduri, G. U. Sumanasekera, Z. Chen, and M. K. Sunkara, *J. Nanosci. Nanotechnol.* 8, 3153 (2008).
19. S. Foss, T. G. Finstad, A. Dana, and A. Aydinli, *Thin Solid Films* 515, 6381 (2007).
20. D. Barba, F. Martin, J. Demarche, G. Terwagne, and G. G. Ross, *Nanotechnology* 23, 145701 (2012).
21. M. Zhang, R. Cai, Y. Zhang, C. Wang, Y. Wang, G. G. Ross, and D. Barba, *Mater. Charact.* 93, 1 (2014).
22. J. F. Ziegler, M. D. Ziegler, and J. P. Biersack, *Nucl. Instrum. Methods B* 268, 1818 (2010).
23. D. Barba, J. Demarche, F. Martin, G. Terwagne, and G. G. Ross, *J. Appl. Phys.* 114, 074306 (2013).
24. D. Barba, R. Cai, J. Demarche, Y. Wang, G. Terwagne, F. Rosei, F. Martin, and G. G. Ross, *Appl. Phys. Lett.* 104, 111901 (2014).
25. Y. Wang, G. G. Ross, and R. Smirani, *Nanotechnology* 15, 1554 (2004).

Received: 17 November 2015. Accepted: 24 February 2016.